NANO LETTERS

2007
Vol. 7, No. 2
403−408

Far-Field Optical Superlens

Zhaowei Liu, Stéphane Durant, Hyesog Lee, Yuri Pikus, Nicolas Fang, Yi Xiong, Cheng Sun, and Xiang Zhang*

NSF Nanoscale Science and Engineering Center (NSEC), 5130 Etcheverry Hall, University of California, Berkeley, California 94720

Received November 9, 2006; Revised Manuscript Received December 19, 2006

ABSTRACT

Far-field optical lens resolution is fundamentally limited by diffraction, which typically is about half of the wavelength. This is due to the evanescent waves carrying small scale information from an object that fades away in the far field. A recently proposed superlens theory offers a new approach by surface excitation at the negative index medium. We introduce a far-field optical superlens (FSL) that is capable of imaging beyond the diffraction limit. The FSL significantly enhances the evanescent waves of an object and converts them into propagating waves that are measured in the far field. We show that a FSL can image a subwavelength object consisting of two 50 nm wide lines separated by 70 nm working at 377 nm wavelength. The optical FSL promises new potential for nanoscale imaging and lithography.

The discovery of Ernst Abbe in 1873 set the fundamental far-field resolution limit for an optical lens known as the "diffraction limit", which typically is about half a wavelength.[1,2] Although shorter wavelength electron beams and X-ray sources have improved resolving power,[3,4] the diffraction limit remains a formidable barrier. Near-field scanning optical microscopy (NSOM) forms images by scanning a sharp tip in close proximity to an object. The near-field profile is thus collected "point-by-point", which is a rather slow process that is incapable of projecting real-time images in the way lenses do.[5−7] Other techniques, based on nonlinear optical effects, have been proposed to improve resolution.[8] Recently, stimulated emission depletion fluorescence microscopy has emerged as one of the most successful techniques for subdiffraction-limited imaging, which cleverly uses saturation transitions between energy states of a fluorescence dye immersed in the object in shaping a subdiffraction spot.[9] However, this approach also requires time-consuming scanning of the object, in addition to the use of dyes and high illumination intensities to achieve the necessary nonlinear response. Recently, a remarkable perfect lens concept has been proposed that has the potential to recover lost evanescent information.[10] This is accomplished by coupling evanescent waves from the object to surface excitations on a slab of negative refractive index material. The lens compensates for evanescent wave decay in free space using the strong enhancement provided by the surface excitations, thereby restoring the evanescent components and projecting a perfect image. This effect has been studied for a wide range of frequencies in both composite metamaterials[11−14] and photonic band gap crystals.[15−18] Recently, optical superlensing has been successfully demonstrated using a silver[19] or SiC slab.[20] However, the superlenses experimentally demonstrated so far are only capable of projecting an image in the near field; due to the intrinsic losses, a simple slab superlens is "near-sighted".[21] Far-field imaging with a superlens still remains a great challenge to many exciting applications. In this Letter, we demonstrate a far-field superlens (FSL) concept with subdiffraction-limit resolution.

The proposed FSL is made of a slab superlens with periodic corrugations.[22] Positioning of a FSL in the vicinity of an object results in significant enhancement of the evanescent waves scattered by the object. The enhanced evanescent components are then converted into propagating waves by a periodic corrugation. As an example, we show a silver superlens with a subwavelength grating in Figure 1a. The evanescent waves scattered from the object are coupled to collective electron oscillations on the metal surface, namely, the surface plasmon (SP), resulting in a significant field enhancement. Combining the FSL with a regular optical microscope, simulation shows that a subdiffraction-limited object can be clearly imaged in the far field (Figure 1b,c).

Subwavelength gratings can be used to convert evanescent waves into propagating waves by shifting their incident field wavevectors, k_{in}, into the various diffraction orders, i.e., $k = k_{in} \pm mk_{\Lambda}$, where $k_{\Lambda} = 2\pi/\Lambda$, m is the diffraction order, and Λ is the grating period.[2] The far-field signal at a given k is therefore a superposition of the various diffraction orders of waves. For example, incident waves with wavevectors k_1, k, and k_2 can be simultaneously mapped into a single propagating wave through the -1, 0, and $+1$ diffraction orders, respectively (Figure 2a). This many-to-one "wavevector mixing" makes the unique retrieval of the original evanescent components impossible, which is why a

* Corresponding author. E-mail: xiang@berkeley.edu.

10.1021/nl062635n CCC: $37.00
Published on Web 01/17/2007

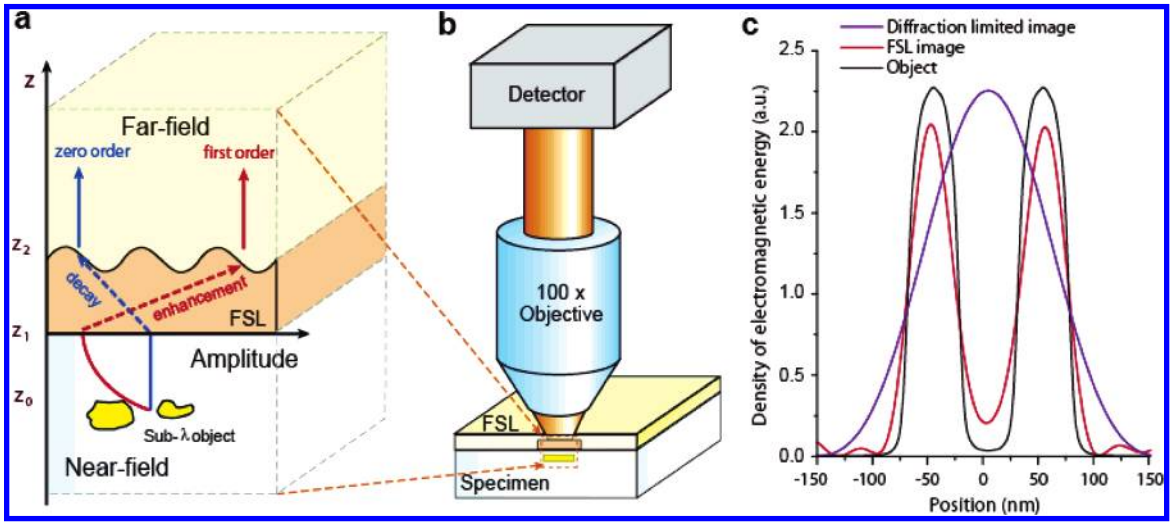

Figure 1. Far-field superlens (FSL) for subwavelength imaging. (a) A FSL is constructed by adding a subwavelength grating onto a thin silver slab. It has two major functions: first, it selectively enhances the evanescent waves from the object; second, it converts evanescent wave into propagating waves. (b) Far-field superlens optical microscope can be realized by insertion of a FSL between the specimen and objective of a regular optical microscope. (c) Subwavelength object with two line sources of 50 nm width separated by a 50 nm gap and its far-field image by FSL calculated for p-polarized normally incident laser light at a wavelength of 377 nm. Calculation shows a unique subdiffraction-limited image can be obtained by FSL. A diffraction limited image from a conventional optical microscope (NA = 1.5) is also shown as comparison.

standard grating configuration fails to form an image in the far field.[23] Earlier efforts were made to increase the numerical aperture of an optical system when a one-dimensional object was imaged by misalignment of the two gratings.[24] This method however, only dealt with propagation waves that resulted in a diffraction-limited image. By contact of the two gratings, recent work shows it is possible to image the subwavelength periodical grating;[25] however, it is inherently limited to a one-dimensional periodical object. Additionally, because of the very low coupling efficiency between two gratings for evanescent waves, the object grating has to be periodic in order to obtain a larger value at specific angular momentum and also has to be physically contacted with another grating. Therefore it cannot provide a general far field imaging method.

We designed a general FSL with unique optical transfer function (OTF) that enables the unambiguous imaging at far field.[22] The OTF, which measures the field ratios before and after the FSL, has the following two special characteristics: a negligible coupling to diffraction orders other than the first and strongly enhanced the first-order OTF over a band of wavevectors, as shown in Figure 2a. By such an ideal transfer function, one can unambiguously map an evanescent band into the propagating band. For example, the far-field radiation at a given k may now consist of only two evanescent components, k_1 and k_2. When examined in conjunction with an ideal design of OTF (red line in Figure 2a), the contribution of k_1 into the far field is negligible, ensuring that only the k_2 component scatters into the propagating mode. Such a one-to-one relationship ensures an unambiguous image for the subwavelength details.

At optical frequencies, metals can support the excitation of surface plasmons. The electromagnetic field enhancement facilitated by SPs is wavevector dependent as a result of an intriguing interplay between the SP modal dispersion and radiative and intrinsic metal losses.[26−28] Such a wavevector dependence can be used for designing a FSL with OTF that closely satisfies the requirements detailed above. We have designed a silver FSL, illustrated in Figure 2b, that maximizes the first order of diffraction for the evanescent component while minimizing the rest. Such OTF selectivity is accommodated by two unique properties of metals. First, SP modes with large k vectors, corresponding to higher diffraction orders, are inherently lossy, resulting in very low transmission. Second, the zero-order transmission can be substantially reduced through the FSL's design.

The FSL geometrical parameters, shown in Figure 2b, are optimized using rigorous coupled wave analysis (RCWA).[29] The calculated OTF in Figure 2c shows that the FSL can indeed significantly enhance evanescent waves and effectively couple them into the far field by predominantly first-order diffraction. The permittivity of silver is taken from the literature,[30] and the refractive index of PMMA is 1.52. The zero-order diffraction is suppressed, as shown by the green curve in Figure 2c. The unambiguous retrieval of evanescent waves is possible over $2.8k_0 < |k| < 4k_0$ (green bars). The lower end points of the retrieval bands are determined from the requirement that the ratio between the OTF for -1 and $+1$ orders should be larger than e. This condition assures that wavevector mixing between these two components is minimized. By applying grazing angle or structured illumination, it is possible to cover the gap of $1.5-2.8k_0$.[31] Combining these techniques with FSL provides a continuous and larger band of wavevectors ($|k| \leq 4k_0$), capable of resolving object features as small as $\lambda_0/8$. As a comparison, a typical oil immersion optical microscope is limited by $|k| \leq 1.5k_0$. The FSL clearly enables the resolution at the subdiffraction limit.

We should note that even though a FSL can project high-resolution information into the far field, it has to be physically

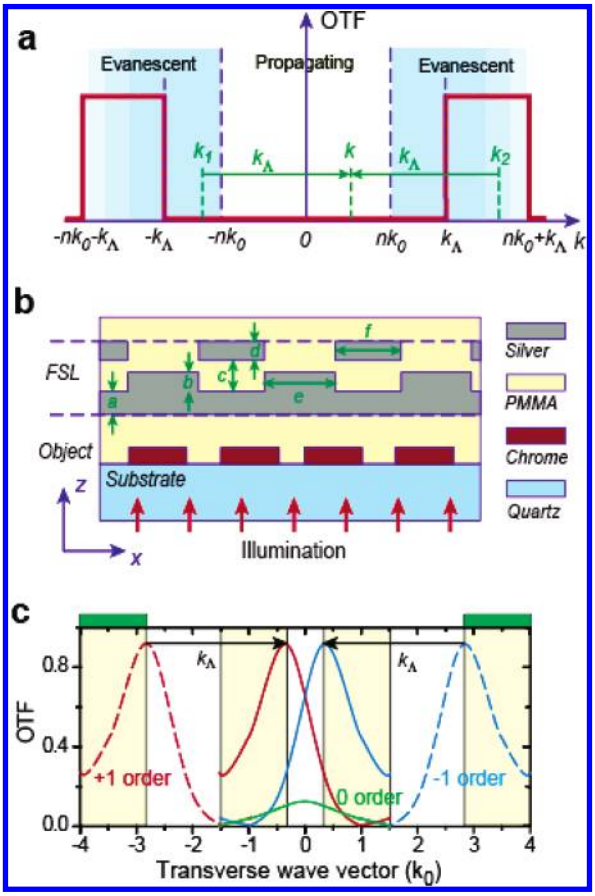

Figure 2. (a) Ideal OTF for FSL that enhances incident evanescent waves within wavevector bands ($nk_0 < |k| < nk_0 + k_\Lambda$) where n is the refractive index of the surrounding media and k_0 and k_Λ are the light wavevector in vacuum and grating wavevector, respectively. This ideal OTF ensures a one-to-one relationship between the measured far-field signal (k) and its evanescent origin (k_2), therefore unique imaging retrieval. (b) Schematic of a silver FSL and a chromium object fabricated on a quartz substrate. The computationally optimized geometry of the FSL is $a = 35$ nm, $b = d = 55$ nm, $c = 100$ nm, $e = 45$ nm, and $f = 105$ nm. (c) Calculated OTF of the optimized FSL under p-polarized incident light with vacuum wavelength of 377 nm and grating wavevector $k_\Lambda = 2.5k_0$. The dashed red and blue curves represent the enhanced evanescent waves. Solid curves represent the propagating waves shifted from the evanescent waves. No wavevector mixing occurs in the shaded range ($2.8k_0 < |k| < 4k_0$) that ensures unique imaging resolution up to $4k_0$.

placed in the near field of an object. The evanescent waves from the object have to reach the FSL before their vanishing thus assures the proper functionalities of a FSL. From this point of view, FSL and NSOM share the same intrinsic limitation. However, the working principle of a FSL, and thus the performance, is completely different with NSOM. A FSL converts evanescent waves into propagating waves in a controllable fashion, i.e., "one-to-one" wavevector conversion. This is the essence of a projection lens, which enables a FSL to directly project a frame of image into the far field. A sharp tip of a NSOM, on the other hand, only scatters localized light out of the near field. A scanning process, therefore, has to be associated to form a real image.

We performed experiments using FSL and a one-dimensional chromium subwavelength nanowire array as an object. The object was inscribed by a focused ion beam (FIB, Strata 201XP) and has a thickness of 40 nm. Six objects are fabricated with periodicities of 120, 130, 140, 160, 180, and 200 nm, respectively. A 35 nm thick spacer of poly(methyl methacrylate) (PMMA) was planarized between the object and the FSL. The silver FSL was then fabricated by thin film depositions and e-beam lithography. The far-field images were obtained by placing the combined object−FSL sample under an optical microscope (Zeiss Axiovert mat 200, 100× oil immersion objective, NA = 1.4). The sample was illuminated by normally incident, p-polarized laser light at 377 nm wavelength (coherent RADIUS 375-8). The far-field images were recorded using a UV-sensitive CCD camera (Princeton Instruments VersArray 1300F).

It can be clearly seen that the FSL projects distinctive fringe images for each object (Figure 3a). The periodicity of the fringe images in the far field increases for objects with characteristic sizes that approach the period of the FSL grating ($\Lambda = 150$ nm). This effect is similar to Moiré fringes but occurs in the near-field zone. The fringe period, δ, is inversely proportional to the difference between the object's evanescent wavevectors and that of the FSL grating: $\delta = 2\pi/\Delta k$, where $\Delta k = |k_{obj} - k_\Lambda|$. For example, an object with a 120 nm spatial period projects far-field fringes with $\delta =$ 600 nm. Thus, using this far-field superlens optical microscope, we showed far-field imaging of objects below the diffraction limit of the conventional optical microscope ($\lambda/$NA $\sim$ 270 nm). In support of these observations, the measured OTF agrees well with the RCWA calculations (Figure 3b). The error bar represents the variation for each sample along the x-axis. A strong wavevector-dependent enhancement of the first order is observed, ensuring an FSL resolution up to $4k_0$. Additional calculations are performed by replacing the silver slab with dielectric PMMA of the same thickness while leaving the metallic grating of FSL in place, and we found, under p-polarization, a very low OTF (blue solid curve). We further observed that, without a silver slab (lower insert compared to the upper one in Figure 3b), a simple grating cannot form an image in the far field that represents the subdiffraction-limited features due to the diminished evanescent field before reaching the grating.

We also performed a control experiment on the same FSL (Figure 3d). Under s polarization, SP excitation on the FSL's surface is not permitted, and thus evanescent wave enhancement does not occur. The distance between the FSL and object is 35 nm, which is about the decay length of the evanescent waves. The evanescent components rapidly diminish over 70 nm distance before reaching the grating of FSL to be converted to the far field, resulting in an image with no features beyond the diffraction limit. The far-field superlens optical microscope images show that the fringe pattern typical for the p polarization (Figure 3c) is absent under s-polarized light (Figure 3d). This is also confirmed in the Fourier spectra. For p polarization, two well-defined symmetric peaks can be seen around $0.4k_0$, corresponding to the object's evanescent field at $2.9k_0$ (Figure 3c); no such response is observed for s polarization (Figure 3d). This demonstrates that the SP enhancement of the evanescent

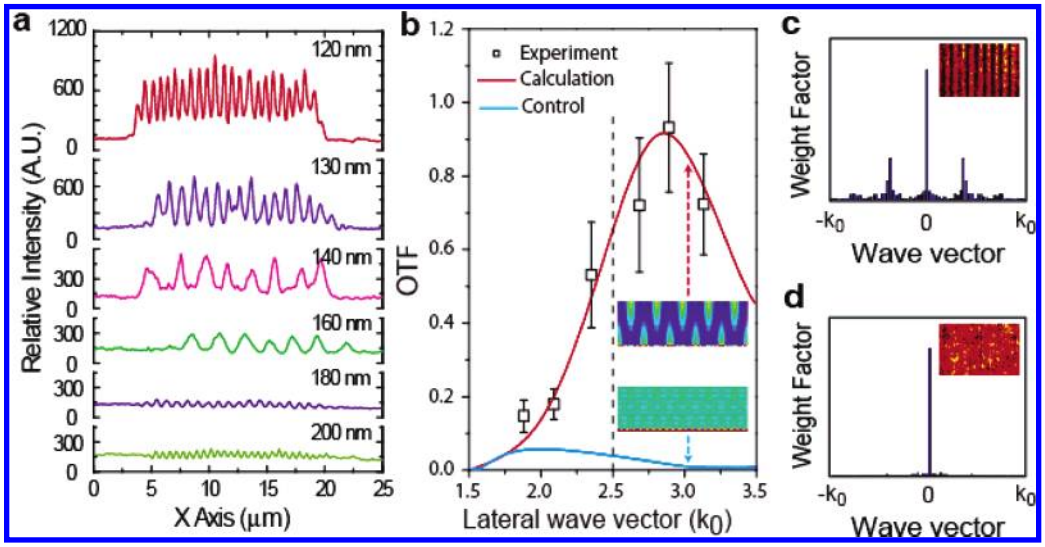

Figure 3. Experimental imaging results of periodic subwavelength objects. (a) Far-field intensity profiles (averaged along fringes) of six nanowire array objects under p-polarized normal illumination at 377 nm. (b) Measured OTF of the silver FSL shows a selectively enhanced band that agrees well with the theoretical calculations (red solid curve). The calculation of a simple grating by replacing the silver slab with PMMA (blue solid curve) shows a very low OTF due to the absence of evanescent wave enhancement. The upper and lower insets compare the computed field distribution after a subwavelength object with FSL and with the simple grating without silver slab, respectively (the object with 120 nm period, i.e., $k \sim 3.14k_0$). A clear image can be seen from the FSL sample at the far field due to the strong evanescent enhancement via silver slab, while no such image is obtained with a simple grating. (c,d) Measured far-field patterns (inset) and their Fourier spectra for the 130 nm object under p and s polarization, respectively. As a control experiment, s polarization does not undergo the surface plasmon mediated enhancement at the FSL, resulting in no characteristics of the object at far field.

waves on the metal slab is one of the key factors enabling the far-field superlens optical imaging with a subdiffraction limit.

As a simple example to show the imaging of an arbitrary object, we use a pair of line objects of 50 nm width with a 70 nm gap (Figure 4a). This line pair object has a broad Fourier spectrum within the limit where silver FSL operates (SOM). As expected, optical imaging through a conventional optical microscope cannot resolve the line pairs due to the diffraction limit (Figure 4b). For FSL imaging, a typical image processing procedure was employed on the pattern captured by the CCD (SOM). First, the Fourier spectrum of the image at CCD was obtained. Because of a slight misalignment between the object and FSL, the first-order diffraction from the FSL can be determined, which is then unfolded back to its original location. The real space image was finally obtained by the second Fourier transformation on the unfolded spectrum. Because s polarization does not excite the surface plasmons at FSL, evanescent waves from the object decay rapidly and become negligible after FSL, leaving only propagation components that result in a diffraction-limited image similar to that from a conventional optical microscope image (Figure 4c). In contrast, for p polarization, the evanescent waves from the object gain significant enhancement by the excitation of surface plasmon in the silver superlens and subsequently are converted into measurable propagating waves at the far field. By combination of the evanescent components from the p polarization with the propagating components from s polarization, the pair of lines of 50 nm width can be clearly imaged (Figure 4d). The FSL image cross section profiles are compared with those obtained from a regular optical microscope and control experiment using s polarization (Figure 4e). The data were averaged along the length of the wires. This strong polarization dependence further confirms that the surface plasmon assisted evanescent wave enhancement plays the key role in the FSL. Using the same method, we have also successfully imaged a three-line object with similar dimensions (SOM). The image processing procedure used here is rather straightforward compared with that used in MRI and X-ray crystallography. In fact, *direct* FSL imaging without postimaging processing can also be performed by using all optical hardware after FSL such as beam splitters, lens, and gratings. Combining both s and p polarizations, FSL can capture simultaneously both propagation and evanescent bands in a single measurement with full bandwidth of $4k_0$ and project a subdiffraction image that allows real-time imaging. Though we showed here imaging of a two-line object as a simple example to demonstrate the concept, general FSL imaging is not limited to one-dimensional objects and has the potential to be used for more complex 2D imaging.

In our proof-of-concept experiment, an object sample combined with a FSL was used. The distance between the object and the FSL can be precisely controlled in nanometer scale by a spacer layer. In practice, the object is detached from the FSL. However, one can always bring the object in the near-field of the FSL by adopting some special techniques. For instance, people have utilized pressure to bring the two pieces into contact.

Another thing we want to mention is the working wavelength. Because we know that the spectacular properties of a FSL are essentially assisted by a broad band surface plasmon excitation on the FSL and we also know that the surface plasmon mode is determined by the material properties from both the metal and the dielectric so that the working wavelength of a FSL can be tuned by changing either the

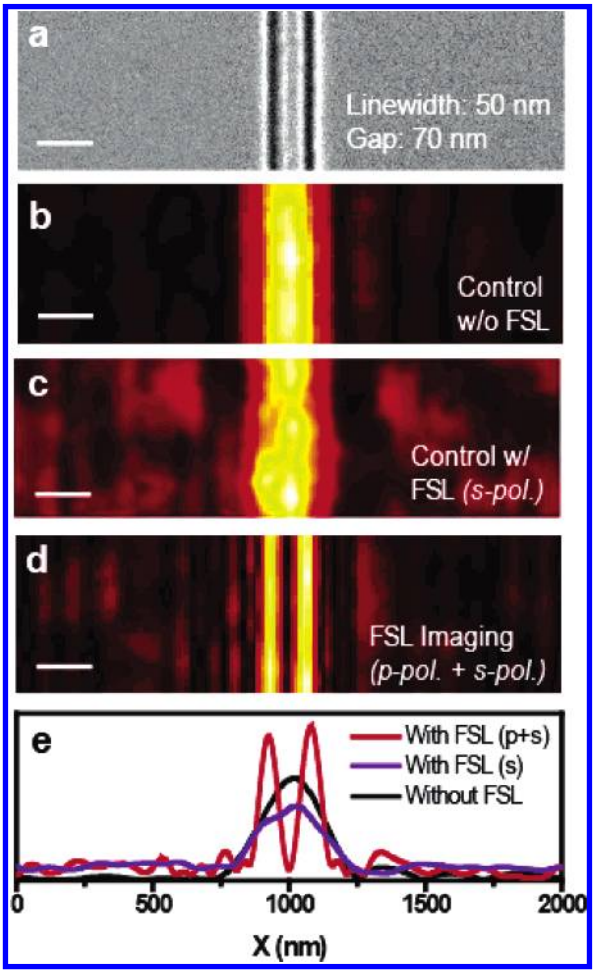

Figure 4. Far-field imaging of a pair of nanowires. (a) Scanning electron microscopy image of an object nanowire pair with 50 nm wide slit and 70 nm gap inscribed by focused ion beam on a 40 nm thick Cr film on the quartz substrate. (b) Diffraction-limited image from a conventional optical microscope cannot resolve the two nanowires (NA = 1.4, λ_0 = 377 nm). (c) Reconstructed FSL images using s polarization is diffraction limited due to the lack of surface plasmon assisted evanescent enhancement. (d) FSL image combining both s and p polarizations that resolves the subdiffraction objects due to strong evanescent enhancement via surface plasmon excitation at FSL. The scale bars in (a), (b), (c), and (d) are 200 nm. (e) The averaged cross-section image profiles from (b), (c), and (d), respectively.

metal or the dielectric. For example, the working wavelength of a silver-structured FSL can move to visible range if a very high refractive index dielectric is used. We will describe the details of designing a visible FSL elsewhere.

The essential function of imaging devices lies in its ability to convert the larger wavevector information to a smaller one that can be detected either optically or electronically. Optical microscopes, for example, use lenses to magnify the micrometer scale features to millimeter size that is visible to the human eye. Transmission electron microscopes, on another hand, by using electrons that have a shorter wavelength, magnify objects down to the nanometer range. In a similar manner, the superlens takes advantage of the short wavelength of surface plasmons and effectively enables one to image at subdiffraction limit. The superlens imaging has been recently demonstrated in the near field,[19,20] and now it is further shown at far field. Though a silver far-field superlens concept is demonstrated here, a more practical and better performing far field superlens microscope can be realized by further development of negative materials. Producing flawless images has been a lens maker's aspiration for many decades. The far-field superlens optical imaging has great potential for many exciting applications in optical imaging, electronics manufacturing, and biomedical sensing.

Acknowledgment. We thank D. Genov and Q.-H Wei for their assistances in manuscript preparation. This research is supported by the Center for Scalable and Integrated Nanomanufacturing (SINAM), an NSF Nanoscale Science and Engineering Center (NSEC) under award no. DMI-0327077, and Office of Naval Research (ONR)/Defense Advanced Research Projects Agency Multidisciplinary University Research Initiative (MURI) (ONR grant N0014-01-1-0803).

Supporting Information Available: Detail of sample fabrication, measurement of the FSL amplitude transfer function, control experiments, and imaging reconstruction. This material is available free of charge via the Internet at http://pubs.acs.org.

References

(1) Abbe, E. *Arch. Mikroskop. Anat.* **1873**, *9*, 413−420.
(2) Born, M.; Wolf, E. *Principles of Optics*, 4th ed.; Pergamon Press: New York, 1970.
(3) Haider, M.; Uhlemann, S.; Schwan, E.; Rose, H.; Kabius, B.; Urban, K. *Nature* **1998**, *392*, 768−769.
(4) Chao, W.; Harteneck, B. D.; Liddle, J. A.; Anderson, E. H.; Attwood, D. T. *Nature* **2005**, *435*, 1210−1213.
(5) Betzig, E.; Trautman, J. K.; Harris, T. D.; Weiner, J. S.; Kostelak, R. K. *Science* **1991**, *251*, 1468−1470.
(6) Courjon, D. *Near-Field Microscopy and Near-Field Optics*; Imperial College Press: London, 2003.
(7) Paesler, M. A.; Moyer, P. J.; Jahncke, C. J.; Johnson, C. E.; Reddick, R. C.; Warmack, R. J.; Ferrell, T. L. *Phys. Rev. B* **1990**, *42*, 6750−6753.
(8) Hell, S. W.; Wichmann, J. *Opt. Lett.* **1994**, *19*, 780−782.
(9) Hell, S. W. *Nat. Biotechnol.* **2003**, *21*, 1347−1355.
(10) Pendry, J. B. *Phys. Rev. Lett.* **2000**, *85*, 3966−3969.
(11) Parazzoli, C. G.; Greegor, R. B.; Koltenbah, B. E. C.; Tanielian, M. *Phys. Rev. Lett.* **2003**, *90*, 107401.
(12) Houck, A. A.; Brock, J. B.; Chuang, I. L. *Phys. Rev. Lett.* **2003**, *90*, 137401.
(13) Grbic, A.; Eleftheriades, G. V. *Phys. Rev. Lett.* **2004**, *92*, 117403.
(14) Cai, W.; Genov, D. A.; Shalaev, V. M. *Phys. Rev. B* **2005**, *72*, 193101.
(15) Notomi, M. *Phys. Rev. B* **2000**, *62*, 10696−10705.
(16) Luo, C.; Johnson, S. G.; Joannopoulos, J. D.; Pendry, J. B. *Phys. Rev. B* **2003**, *68*, 045115.
(17) Parimi, V. P.; Lu, W. T.; Vodo, P.; Sridhar, S. *Nature* **2003**, *426*, 404−404.
(18) Cubukcu, E.; Aydin, K.; Ozbay, E.; Foteinopolou, S.; Soukoulis, C. M. *Phys. Rev. Lett.* **2003**, *91*, 207401.
(19) Fang, N.; Lee, H. S.; Sun, C.; Zhang, X. *Science* **2005**, *308*, 534−537.
(20) Taubner, T.; Korobkin, D.; Urzhumov, Y.; Shvets, G.; Hillenbrand, R. *Science* **2006**, *313*, 1595.
(21) Podolskiy, V. A.; Narimanov, E. E. *Opt. Lett.* **2005**, *30*, 75−77.
(22) Durant, S.; Liu, Z.; Fang, N.; Zhang, X. www.arxiv.org, **2006**, physics/0601163. Durant, S.; Liu, Z.; Steele, J. M.; Zhang, X. *J. Opt. Soc. Am. B* **2006**, *23*, 2383−2392.
(23) Evanescent wave limited superresolution is achievable based on two moving gratings as described in the following paper: Lukosz, W. *J. Opt. Soc. Am.* **1967**, *57*, 932−941.

(24) Grimm, M. A.; Lohmann, A. W. *J. Opt. Soc. Am.* **1966**, *56*, 1151−1156.
(25) Eckhouse, V.; Zalevsky, Z.; Konforti, N.; Mendlovic, D. *Opt. Eng.* **2004**, *43*, 2462−2468.
(26) Raether, H. *Surface Plasmons on Smooth and Rough Surfaces and on Gratings*; Springer-Verlag: Berlin, 1988.
(27) Barnes, W. L.; Dereux, A.; Ebbesen, T. W. *Nature* **2003**, *424*, 824−830.
(28) Liu, Z.; Fang, N.; Yen, T. J.; Zhang, X. *Appl. Phys. Lett.* **2003**, *83*, 5184−5186.
(29) Moharam, M. G.; Grann, E. B.; Pommet, D. A.; Gaylord, T. K. *J. Opt. Soc. Am. A* **1995**, *12*, 1068−1076.
(30) Johnson, P. B.; Christy, R. W. *Phys. Rev. B* **1972**, *6*, 4370−4379.
(31) Gustafsson, M. G. L. *J. Microsc.* **2000**, 198. 82−87.

NL062635N